Reduced cross sections of electron and neutrino charged current quasielastic scattering on nuclei

A. V. Butkevich
Institute for Nuclear Research, Russian Academy of Sciences, Moscow 117312, Russia

(Received 6 November 2023; accepted 28 March 2024; published 23 April 2024)

The semiexclusive averaged reduced cross sections for (anti)neutrino charged current quasielastic scattering on carbon, oxygen, and argon are analyzed within the relativistic distorted wave impulse approximation. One finds that these cross sections as functions of missing nucleon energy are similar to those of electron scattering and are in agreement with electron scattering data for the three nuclei. The difference between the electron and neutrino cross sections can be attributed to Coulomb distortion on the electron wave function. The averaged reduced cross sections depend slowly upon incoming lepton energy. The approach presented in this paper provides novel constraints on nuclear models of quasielastic neutrino-nucleus scattering and can be easily applied to test spectral functions and final state interactions employed in neutrino event generators.

DOI: 10.1103/PhysRevC.109.045502

I. INTRODUCTION

For current [1,2] and future [3–5] accelerator-based neutrino experiments the primary physics goals are measuring the lepton $\mathcal{CP}$ violation phase, determining neutrino mass ordering, and testing the three-flavor paradigm. In these experiments to evaluate the oscillation parameters, the probabilities of neutrino oscillations as functions of neutrino energy are measured. The neutrino beams are not monoenergetic and have broad distributions that range from tens of MeV to a few GeV. The accuracy to which neutrino oscillation parameters can be extracted depends on the ability of experiments to determine the individual energy of a detected neutrino.

Measurements at neutrino energy 1 GeV are critical for the T2K [2] and HK [4] programs, which are carbon and water (oxygen) detectors, as well as for the SBN (argon) [5] program. Measurements from 1 to 2 GeV are important for the NOvA (carbon, chlorine) [1] experiment, and measurements spanning from 1 to 10 GeV are critical for the DUNE (argon) [3] program. At GeV-scale neutrino energies the neutrino can interact with a nucleus through a wide range of reaction channels. These include charged-current (CC) quasielastic (QE) scattering, two-body meson exchange current (MEC) channels, resonance production, and deep inelastic scattering.

The incident neutrino energy is reconstructed using kinematic or calorimetric methods. At energy about 1 GeV, where the CCQE scattering is dominant, the incoming neutrino energy can be derived from lepton kinematics alone. The calorimetric method relies not only on the visible energy measured in the detector, but also on the models of the neutrino-nucleus interactions that are implemented in neutrino event generators. In addition the neutrino-nucleus scattering model is critical for obtaining background estimates and for correct extrapolations of the near detector constraints to the far detector in analyses aimed at determining the neutrino oscillation parameters.

Unfortunately, due to wide range of neutrino energy beams and poor statistics available from current experiments, it is very difficult to measure differential neutrino-nucleus cross sections for specific energies and to test beam energy reconstruction techniques. On the theoretical side, many studies have been presented aiming at improving knowledge of lepton-nucleus interaction [6–27]. However, it is extremely challenging to provide reliable and consistent predictions for the diversity of processes that can take place in the energy range covered by the neutrino beams. Various contributions to the cross sections can significantly overlap with each other, making it difficult to identify, diagnose, and remedy shortcoming of nuclear models.

While electron and neutrino interactions are different at the primary vertex, many underlying physics process in the nucleus are the same, and electron scattering data collected with precisely controlled kinematics (initial and final energies and scattering angles) and large statistics allow validation and improvement of the description of nuclear effects. There is a large body of electron-scattering data on carbon and calcium, and only a few data sets are available for scattering on argon.

All of the above reaction mechanisms are very similar for electrons and for neutrinos. From the nuclear point of view the influence of nuclear medium effects such as the nuclear ground state and interaction of the outgoing nucleon with the residual nucleus can be expected to be largely the same for electron as for neutrino-induced processes. It is possible to exploit this similarity and use electron scattering data with known beam energies to test the neutrino energy reconstruction methods [28] and interaction models. The vector part of the electroweak interaction can be inferred directly from

the electron scattering data. Because electron and neutrino scattering are strongly linked in theory, any model of neutrino interactions (vector+axial) should also be able to reproduce electron (vector) interactions. A model unable to reproduce electron measurements cannot be expected to provide accurate predictions for neutrino cross sections.

It is therefore unsurprising that recent years have seen a plethora of analyses of electron-scattering data to test the vector current part of the lepton-nucleus interaction against existing inclusive electron scattering cross sections for different target nuclei at several incident beam energies and scattering electron angles. The relativistic distorted wave impulse approximation (RDWIA), initially designed for description of exclusive $(e, e'p)$ data [29–31] and then adopted for neutrino reactions, was successfully tested against inclusive (e, e') data [23,24]. The SuSAv2 model exploits the similarities between both interaction types to guide the description of the weak scattering process [16,17]. The utility of validating neutrino events generators against inclusive electron scattering data that they had not been tuned to was demonstrated in Refs. [32–35].

Such inclusive reactions involve total hadronic cross sections and typically are relatively insensitive to the details of the final nuclear states. Rather simple models may yield cross sections that are not very different from those found in the most sophisticated models. Typically, the inclusive predictions using different models are rather similar and agree to about 10–20%, but they cannot make predictions on both leptons and hadrons in final states. The semiexclusive $(l, l'p)$ lepton scattering process involves not the total cross sections but the specific asymptotic states, and allows one to test the nuclear model more in detail. Microscopic and unfactorized models like the RDWIA can be used to model both lepton-boson and boson-nucleus vertexes in the same detail and compare the results to semiexclusive observables. The comparison of the results of the RDWIA approach and cascade models employed in the neutrino event generators provides constraints on cascade models from proton-nucleus scattering [36].

The reduced cross section, obtained from the measured differential semiexclusive electron scattering cross section divided by the kinematic factor and the off-shell electron-proton cross section, can be identified with the distorted spectral function. Final state interactions between the ejected nucleon and the residual nucleus make the reduced cross sections depend upon the initial and ejectile nucleons' momenta and angle between them (which depends upon momentum transfer). Thus, irrespective of the type of interaction (electromagnetic or weak) the distorted spectral function is determined mainly by the intrinsic properties of the target and the ejected nucleon interaction with residual nucleus.

The purpose of the present work is calculation of the CCQE neutrino scattering reduced cross sections averaged over phase space as functions of the missing nucleon momentum and incoming neutrino energy, and comparison of them with ones obtained from measurements of $(e, e'p)$ scattering on carbon, oxygen, and argon targets. The direct comparison of the spectral functions used in the factorized approach in neutrino event generators to the measured reduced cross sections of the electron-nucleus scattering can provide an additional test of the nuclear models employed in these generators.

The outline of this paper is the following. In Sec. II the formalism needed to describe the semiexclusive lepton-nucleus CCQE scattering process is presented. The RDWIA model is briefly introduced in Sec. III. Results of the calculations are presented in Sec. IV. Conclusions are summarized in Sec. V.

II. FORMALISM OF QUASIELASTIC SCATTERING

The formalism used to describe electron and neutrino quasi-elastic exclusive scattering,

$$l(k_i) + A(p_A) \to l'(k_f) + N(p_x) + B(p_B), \tag{1}$$

off nuclei in the one-photon (W boson) exchange approximation is considered. Here l labels the incident lepton [electron or muon (anti)neutrino], and l' represents the scattered lepton (electron or muon), $k_i = (\varepsilon_i, \boldsymbol{k}_i)$ and $k_f = (\varepsilon_f, \boldsymbol{k}_f)$ are the initial and final lepton momenta, $p_A = (\varepsilon_A, \boldsymbol{p}_A)$ and $p_B = (\varepsilon_B, \boldsymbol{p}_B)$ are the initial and final target momenta, $p_x = (\varepsilon_x, \boldsymbol{p}_x)$ is the ejectile nucleon momentum, $q = (\omega, \boldsymbol{q})$ is the momentum transfer carried by the virtual photon (W boson), and $Q^2 = -q^2 = \boldsymbol{q}^2 - \omega^2$ is the photon (W boson) virtuality.

A. CCQE lepton-nucleus cross sections

In the laboratory frame the differential cross section for exclusive electron (σ^{el}) and (anti)neutrino (σ^{cc}) CC scattering can be written as

$$\frac{d^6\sigma^{el}}{d\varepsilon_f d\Omega_f d\varepsilon_x d\Omega_x} = \frac{|\boldsymbol{p}_x|\varepsilon_x}{(2\pi)^3}\frac{\varepsilon_f}{\varepsilon_i}\frac{\alpha^2}{Q^4}L^{(\mathrm{el})}_{\mu\nu}\mathcal{W}^{\mu\nu(\mathrm{el})}, \tag{2a}$$

$$\frac{d^6\sigma^{cc}}{d\varepsilon_f d\Omega_f d\varepsilon_x d\Omega_x} = \frac{|\boldsymbol{p}_x|\varepsilon_x}{(2\pi)^5}\frac{|\boldsymbol{k}_f|}{\varepsilon_i}\frac{G^2\cos^2\theta_c}{2}L^{(\mathrm{cc})}_{\mu\nu}\mathcal{W}^{\mu\nu(\mathrm{cc})}, \tag{2b}$$

where Ω_f is the solid angle for the lepton momentum, Ω_x is the solid angle for the ejectile nucleon momentum, $\alpha \simeq 1/137$ is the fine-structure constant, $G \simeq 1.16639 \times 10^{-11}$ MeV^{-2} is the Fermi constant, θ_C is the Cabbibo angle ($\cos\theta_C \approx 0.9749$), $L^{\mu\nu}$ is the lepton tensor, and $\mathcal{W}^{(\mathrm{el})}_{\mu\nu}$ and $\mathcal{W}^{(\mathrm{cc})}_{\mu\nu}$ are respectively the electromagnetic and weak CC nuclear tensors.

For exclusive reactions in which only a single discrete state or a narrow resonance of the target is excited, it is possible to integrate over the peak in missing energy and obtain a fivefold differential cross section of the form

$$\frac{d^5\sigma^{el}}{d\varepsilon_f d\Omega_f d\Omega_x} = R\frac{|\boldsymbol{p}_x|\tilde{\varepsilon}_x}{(2\pi)^3}\frac{\varepsilon_f}{\varepsilon_i}\frac{\alpha^2}{Q^4}L^{(\mathrm{el})}_{\mu\nu}W^{\mu\nu(\mathrm{el})}, \tag{3a}$$

$$\frac{d^5\sigma^{cc}}{d\varepsilon_f d\Omega_f d\Omega_x} = R\frac{|\boldsymbol{p}_x|\tilde{\varepsilon}_x}{(2\pi)^5}\frac{|\boldsymbol{k}_f|}{\varepsilon_i}\frac{G^2\cos^2\theta_c}{2}L^{(\mathrm{cc})}_{\mu\nu}W^{\mu\nu(\mathrm{cc})}, \tag{3b}$$

where R is a recoil factor,

$$R = \int d\varepsilon_x \delta(\varepsilon_x + \varepsilon_B - \omega - m_A) = \left|1 - \frac{\tilde{\varepsilon}_x}{\varepsilon_B}\frac{\boldsymbol{p}_x \cdot \boldsymbol{p}_B}{\boldsymbol{p}_x \cdot \boldsymbol{p}_x}\right|^{-1}, \tag{4}$$

$\tilde{\varepsilon}_x$ is solution to equation $\varepsilon_x + \varepsilon_B - m_A - \omega = 0$, where $\varepsilon_B = \sqrt{m_B^2 + \boldsymbol{p}_B^2}$, $\boldsymbol{p}_B = \boldsymbol{q} - \boldsymbol{p}_x$, and m_A and m_B are masses of the

target and recoil nucleus, respectively. Note that missing momentum is $\boldsymbol{p}_m = \boldsymbol{p}_x - \boldsymbol{q}$ and missing energy ε_m is defined by $\varepsilon_m = m + m_B - m_A$.

All information about the nuclear structure and effects of final-state interaction (FSI) between the ejectile nucleon and residual nucleus is contained in the electromagnetic and weak CC hadronic tensors, $W^{(\mathrm{el})}_{\mu\nu}$ and $W^{(\mathrm{cc})}_{\mu\nu}$, which are given by the bilinear products of the transition matrix elements of the nuclear electromagnetic or CC operator $J^{(\mathrm{el})(\mathrm{cc})}_{\mu}$ between the initial nucleus state $|A\rangle$ and the final state $|B_f\rangle$ as

$$W^{(\mathrm{el})(\mathrm{cc})}_{\mu\nu} = \sum_f \langle B_f, p_x | J^{(\mathrm{el})(\mathrm{cc})}_{\mu} | A \rangle \langle A | J^{(\mathrm{el})(\mathrm{cc})\dagger}_{\nu} | B_f, p_x \rangle, \quad (5)$$

where the sum is taken over undetected states.

In the exclusive reaction (1) the outgoing lepton and proton are detected and the exclusive lepton scattering cross sections (3a) and (3b) in terms of response functions can be written as

$$\frac{d^5\sigma^{el}}{d\varepsilon_f d\Omega_f d\Omega_x} = \frac{|\boldsymbol{p}_x|\tilde{\varepsilon}_x}{(2\pi)^3}\sigma_M R\big(V_L R^{(\mathrm{el})}_L + V_T R^{(\mathrm{el})}_T + V_{LT} R^{(\mathrm{el})}_{LT}\cos\phi + V_{TT} R^{(\mathrm{el})}_{TT}\cos 2\phi\big), \quad (6a)$$

$$\begin{aligned}\frac{d^5\sigma^{cc}}{d\varepsilon_f d\Omega_f d\Omega_x} = \frac{|\boldsymbol{p}_x|\tilde{\varepsilon}_x}{(2\pi)^5} G^2 \cos^2\theta_c \varepsilon_f |\boldsymbol{k}_f| R\{ & v_0 R_0 + v_T R_T \\ & + v_{TT} R_{TT}\cos 2\phi + v_{zz} R_{zz} \\ & + (v_{xz} R_{xz} - v_{0x} R_{0x})\cos\phi - v_{0z} R_{0z} \\ & + h[v_{yz}(R'_{yz}\sin\phi + R_{yz}\cos\phi) \\ & - v_{0y}(R'_{0y}\sin\phi + R_{0y}\cos\phi) - v_{xy} R_{xy}]\},\end{aligned} \quad (6b)$$

where

$$\sigma_M = \frac{\alpha^2 \cos^2\theta/2}{4\varepsilon_i^2 \sin^4\theta/2} \quad (7)$$

is the Mott cross section and h is $+1$ for positive lepton helicity and -1 for negative lepton helicity. The coupling coefficients V_k and v_k, the expressions of which are given in Ref. [6], are kinematic factors depending on the lepton's kinematics. The response functions R_i are given in terms of components of the exclusive hadronic tensors [6] and depend on the variables (Q^2, ω) or $(|\boldsymbol{q}|, \omega)$.

It is also useful define a reduced cross section

$$\sigma_{\mathrm{red}} = \frac{d^5\sigma^{(\mathrm{el})(\mathrm{cc})}}{d\varepsilon_f d\Omega_f d\Omega_x} \Big/ K^{(\mathrm{el})(\mathrm{cc})}\sigma_{lN}, \quad (8)$$

where $K^{\mathrm{el}} = R p_x \varepsilon_x/(2\pi)^3$ and $K^{\mathrm{cc}} = R p_x \varepsilon_x/(2\pi)^5$ are phase-space factors for electron and neutrino scattering and σ_{lN} is the corresponding elementary cross section for the lepton scattering from the moving free nucleon normalized to unit flux. The reduced cross section is an interesting quantity that can be regarded as the nucleon momentum distribution modified by FSI, i.e., as the distorted spectral function. Final-state interactions make the reduced cross sections $\sigma_{\mathrm{red}}(\boldsymbol{p}_m, \boldsymbol{p}_x)$ depend upon ejectile momentum $\boldsymbol{p}_x$, the angle between the initial and final nucleon momenta, and the incident lepton energy. These cross sections for (anti)neutrino scattering off nuclei are similar to those of electron scattering apart from small differences at low beam energy due to effects of Coulomb distortion of the incoming electron wave function, as shown in Refs. [6,7,12]

The factorization approximation to the knockout cross section stipulates that

$$\frac{d^5\sigma^{(\mathrm{el})(\mathrm{cc})}}{d\varepsilon_f d\Omega_f d\Omega_x} = K^{(\mathrm{el})(\mathrm{cc})} \times \sigma_{lN} \times \sigma_{\mathrm{red}}(\boldsymbol{\varepsilon}_m, \boldsymbol{p}_m, \boldsymbol{p}_x). \quad (9)$$

This factorization implies that the initial nuclear sate and FSI effects are decoupled from the leptonic vertex, with preserved correlations between the final lepton and nucleon.

The reduced cross section as a function of missing momentum p_m, averaged over phase volume in (ω, Ω_f, ϕ) coordinates, where $\Omega_x = (\cos\theta_{pq}, \phi)$, can be written as

$$\langle \sigma^{\mathrm{red}}(p_m)\rangle = \frac{1}{V}\int d\phi \int d\boldsymbol{\varepsilon}_f \int d\Omega_f \frac{p_m}{p_x|\boldsymbol{q}|} R_c \sigma^{\mathrm{red}} \times (\boldsymbol{\varepsilon}_f, \Omega_f, p_m, \phi), \quad (10)$$

where $p_m = |\boldsymbol{p}_m|$, $p_x = |\boldsymbol{p}_x|$, $\boldsymbol{p}_m = \boldsymbol{p}_x - \boldsymbol{q}$, and

$$\cos\theta_{pq} = \frac{\boldsymbol{p}_x^2 + \boldsymbol{q}^2 - \boldsymbol{p}_m^2}{2p_x|\boldsymbol{q}|}, \quad (11a)$$

$$R_c = 1 + \frac{\varepsilon_x}{2p_x^2 \varepsilon_B}\big(\boldsymbol{p}_x^2 + \boldsymbol{q}^2 - \boldsymbol{p}_m^2\big), \quad (11b)$$

$$V = \int d\phi \int d\boldsymbol{\varepsilon}_f \int d\Omega_f \frac{p_m}{p_x|\boldsymbol{q}|} R_c. \quad (11c)$$

Precise electron reduced cross sections data can be used to validate the neutrino reduced cross sections (spectral functions) that are implemented in neutrino generators.

B. Nuclear current

Obviously, the determination of the response tensor $W^{\mu\nu}$ requires knowledge of the nuclear current matrix elements in Eq. (5). The lepton-nucleon scattering is described in the impulse approximation, assuming that the incoming lepton interacts with only one nucleon, which is subsequently emitted. The nuclear current is written as the sum of single-nucleon currents. Then, the nuclear matrix element in Eq. (5) takes the form

$$\langle p, B | J^{\mu} | A \rangle = \int d^3 r \, \exp(i\boldsymbol{t}\cdot\boldsymbol{r}) \overline{\Psi}^{(-)}(\boldsymbol{p}, \boldsymbol{r}) \Gamma^{\mu} \Phi(\boldsymbol{r}), \quad (12)$$

where Γ^{μ} is the vertex function, $\boldsymbol{t} = \varepsilon_B \boldsymbol{q}/W$ is the recoil-corrected momentum transfer, $W = \sqrt{(m_A + \omega)^2 - \boldsymbol{q}^2}$ is the invariant mass, and Φ and $\Psi^{(-)}$ are relativistic bound-state and outgoing wave functions. For electron scattering, most calculations use the CC2 electromagnetic vertex function for a free nucleon [37],

$$\Gamma^{\mu} = F^{(\mathrm{el})}_V(Q^2)\gamma^{\mu} + i\sigma^{\mu\nu}\frac{q_{\nu}}{2m} F^{(\mathrm{el})}_M(Q^2), \quad (13)$$

where $\sigma^{\mu\nu} = i[\gamma^{\mu}\gamma^{\nu}]/2$, and $F^{(\mathrm{el})}_V$ and $F^{(\mathrm{el})}_M$ are the Dirac and Pauli nucleon form factors. Because the bound nucleons are off shell, the vertex Γ^{μ} in Eq. (13) should be taken for an off-shell nucleon.Using the de Forest prescription, the off-shell

vertex can be wrintte as [37]

$$\tilde{\Gamma}^{\mu} = F_V^{(\mathrm{el})}(Q^2)\gamma^{\mu} + i\sigma^{\mu\nu}\frac{\tilde{q}_{\nu}}{2m}F_M^{(\mathrm{el})}(Q^2), \tag{14}$$

where $\tilde{q} = (\varepsilon_x - \tilde{E}, \boldsymbol{q})$ and the nucleon energy $\tilde{E} = \sqrt{m^2 + (\boldsymbol{p}_x - \boldsymbol{q})^2}$ is placed on shell. We use the approximation of [38] on the nucleon form factors. The Coulomb gauge is assumed for the single-nucleon current. Although the experimental analyses usually employ the de Forest CC1 prescription for σ_{lN}, consistency requires that calculation of σ_{red} to employ the σ_{lN} that corresponds to the current operator used in the RDWIA calculations.

The single-nucleon charged current has V-A structure $J^{\mu(\mathrm{cc})} = J_V^{\mu} + J_A^{\mu}$. For a free nucleon vertex function $\Gamma^{\mu(\mathrm{cc})} = \Gamma_V^{\mu} + \Gamma_A^{\mu}$ one uses the CC2 vector current vertex function

$$\Gamma_V^{\mu} = F_V(Q^2)\gamma^{\mu} + i\sigma^{\mu\nu}\frac{q_{\nu}}{2m}F_M(Q^2) \tag{15}$$

and the axial current vertex function

$$\Gamma_A^{\mu} = F_A(Q^2)\gamma^{\mu}\gamma_5 + F_P(Q^2)q^{\mu}\gamma_5. \tag{16}$$

Weak vector form factors F_V and F_M are related to corresponding electromagnetic ones for proton $F_{i,p}^{(\mathrm{el})}$ and neutron $F_{i,n}^{(\mathrm{el})}$ by the hypothesis of conserved vector current (CVC):

$$F_i = F_{i,p}^{(\mathrm{el})} - F_{i,n}^{(\mathrm{el})}. \tag{17}$$

The axial F_A and pseudoscalar F_P form factors in the dipole approximation are parametrized as

$$F_A(Q^2) = \frac{F_A(0)}{(1 + Q^2/M_A^2)^2}, \quad F_P(Q^2) = \frac{2mF_A(Q^2)}{m_{\pi}^2 + Q^2}, \tag{18}$$

where $F_A(0) = 1.2724$, m_{π} is the pion mass, and M_A is the axial mass. The de Forest prescription for off-shell extrapolation of $\Gamma^{\mu(\mathrm{cc})}$ is used. Similarly to electromagnetic current, the Coulomb gauge is applied for the vector current J_V.

III. MODEL

The semiexclusive differential and reduced cross sections for neutrino scattering were studied in Refs. [6,7,12,25,26], using the relativistic shell model approach and taking into account the FSI effects. A formalism for the $A(e, e'N)B$ reaction that describes the channel coupling in the FSI of $N + B$ system was developed in Ref. [31].

In this work the independent particle shell model (IPSM) is assumed for the nuclear structure. The model space for $^{12}\mathrm{C}(l, l'N)$ consists of $1s_{1/2}$ and $1p_{3/2}$ nucleon-hole states in the $^{11}\mathrm{B}$ and $^{11}\mathrm{C}$ nuclei. The model space for $^{16}\mathrm{O}(l, l'N)$ consists of $1s_{1/2}$, $1p_{3/2}$, and $1p_{1/2}$ nucleon-hole states in the $^{15}\mathrm{N}$ and $^{15}\mathrm{O}$ nuclei. The model space for $^{40}\mathrm{Ar}(l, l'N)$ consists of $1s_{1/2}$, $1p_{3/2}$, $1p_{1/2}$, $1d_{5/2}$, $2s_{1/2}$, and $1d_{3/2}$ nucleon-hole states in the $^{39}\mathrm{Cl}$ nucleus, and $1s_{1/2}$, $1p_{3/2}$, $1p_{1/2}$, $1d_{5/2}$, $2s_{1/2}$, $1d_{3/2}$, and $1f_{7/2}$ nucleon-hole states in the $^{39}\mathrm{Ar}$ nucleus. All states in these nuclei are regarded as discrete states even though their spreading widths are actually appreciable.

In the independent particle shell model the relativistic bound-state function Φ in Eq.(12) is obtained as the self-consistent solutions of a Dirac equation, derived within a relativistic mean-field approach, from a Lagrangian containing σ, ω, and ρ mesons [39]. The nucleon bound-state functions were calculated by the TIMORA code [40] with the normalization factors $S(\alpha)$ relative to full occupancy of the IPSM orbitals. According the RDWIA analysis of the JLab $^{12}\mathrm{C}(e, e'p)$ data [41,42] $S(1p_{3/2}) = 84\%$, $S(1s_{1/2}) = 100\%$, and the average factor is $\approx 89\%$. In this work one assumes that the missing strength can be attributed to the short-range nucleon-nucleon (NN) correlations, leading to the appearance

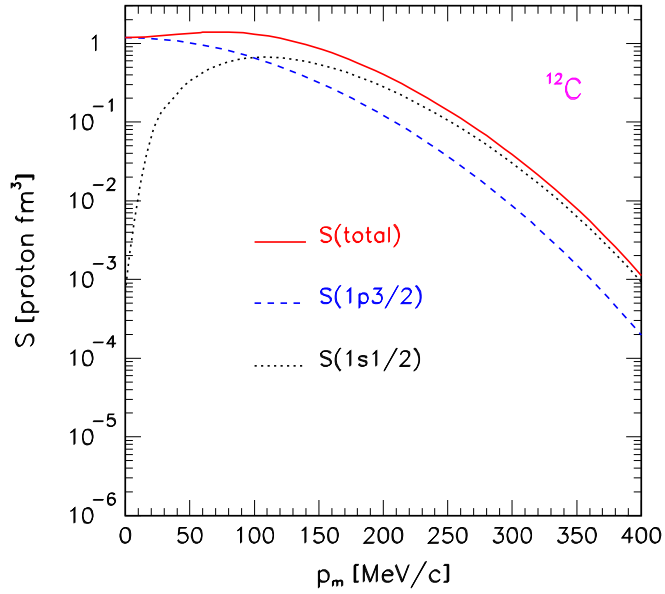

FIG. 1. Proton momentum distributions for the $1p_{1/2}$ (dashed line) and $1s_{1/2}$ (dotted line) single-particle states in the $^{12}\mathrm{C}$ nucleus. Also shown is the total proton momentum distribution (solid line).

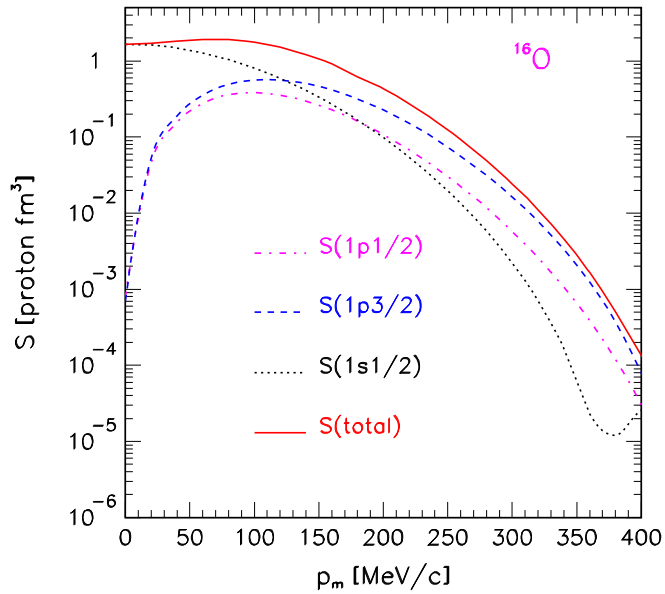

FIG. 2. Same as Fig. 1 but for $1p_{1/2}$ (dashed-dotted line), $1p_{3/2}$ (dashed line), and $1s_{1/2}$ (dotted line) single-particle states in the $^{16}\mathrm{O}$ nucleus.

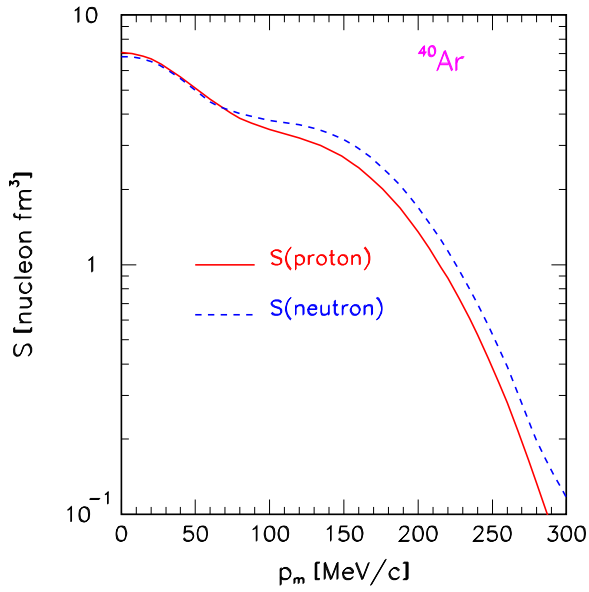

FIG. 3. Total proton and neutron momentum distributions in the ^{40}Ar nucleus.

of the high-momentum and high-energy nucleon distribution in the target. These estimations of the depletion of hole states are consistent with a direct measurement of the spectral function using ^{12}C$(e, e'p)$ in the parallel kinematics [43], which observed approximately 0.6 protons in a region with $p_m \geqslant 240$ MeV$/c$ and $\varepsilon_m \geqslant 50$ MeV, attributable to a single-nucleon knockout from the correlated cluster. Similar estimates of the depletion of hole states are available from the self-consistent Green's function method [44], the correlated basis function theory [45], and other methods. I used the following values of normalization factors of ^{16}O that were obtained in the RDWIA analysis of the JLab data [46]: $S(1p_{3/2}) = 66\%$, $S(1p_{1/2}) = 70\%$, and $S(1s_{1/2}) = 100\%$. From the RDWIA analysis [12] of NIKHEF data [47–49] it follows that the occupancies of the orbitals of ^{40}Ca and ^{40}Ar are approximately 87% on average. Proton and neutron binding energies and the occupancies of the orbitals in ^{40}Ar are given in Table II of Ref. [12].

Figures 1 and 2 show the proton momentum distributions for occupied orbitals in ^{12}C and ^{16}O, calculated within the mean-field approach. The neutron momentum distributions in these nuclei are almost identical to proton ones. The total proton and neutron momentum distributions in ^{40}Ar are presented in Fig. 3. These distributions are normalized to the total number of protons/neutrons in the IPSM shells.

For an outgoing nucleon, the simplest chose is to use plane-wave function Ψ in Eq. (12), that is, there are no interactions between the ejected nucleon N and the residual nucleus B; i.e., to use the so-called plane-wave impulse approximation (PWIA). For a more realistic description, final state interaction effects should be taken into account. In the RDWIA the distorted-wave function of the knocked out nucleon Ψ is evaluated as a solution of a Dirac equations containing a phenomenological relativistic optical potential [46]. This potential consists of a real part, which describes the rescattering of the ejected nucleon, and an imaginary part for the absorption of it into unobserved channels. The LEA program [50] is used for numerical calculation of the distorted-wave function with the EDAD1 parametrization [51] of the relativistic optical potentials for carbon, oxygen, and calcium.

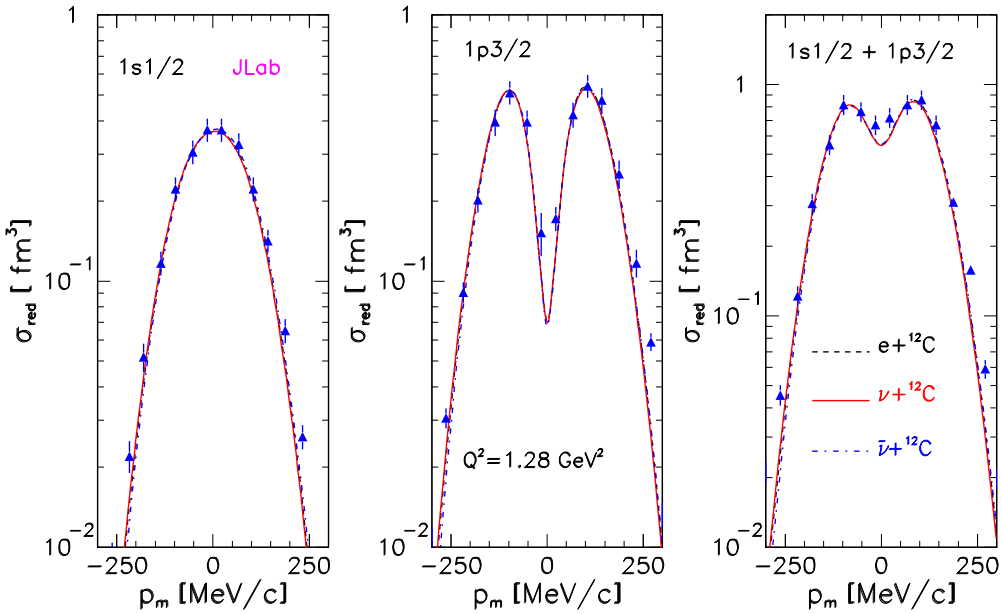

FIG. 4. Comparison of the RDWIA calculations for electron, neutrino, and antineutrino reduced cross sections for the removal of nucleons from $1s$ and $1p$ shells of ^{12}C as functions of the missing momentum. JLab data [41] are for beam energy $E_{\text{beam}} = 2.455$ GeV, proton kinetic energy $T_p = 350$ MeV, and $Q^2 = 0.64$ (GeV$/c)^2$. The RDWIA calculations are shown for electron scattering (dashed line) and neutrino (solid line) and antineutrino (dashed-dotted line) scattering. This figure was taken from Ref. [7].

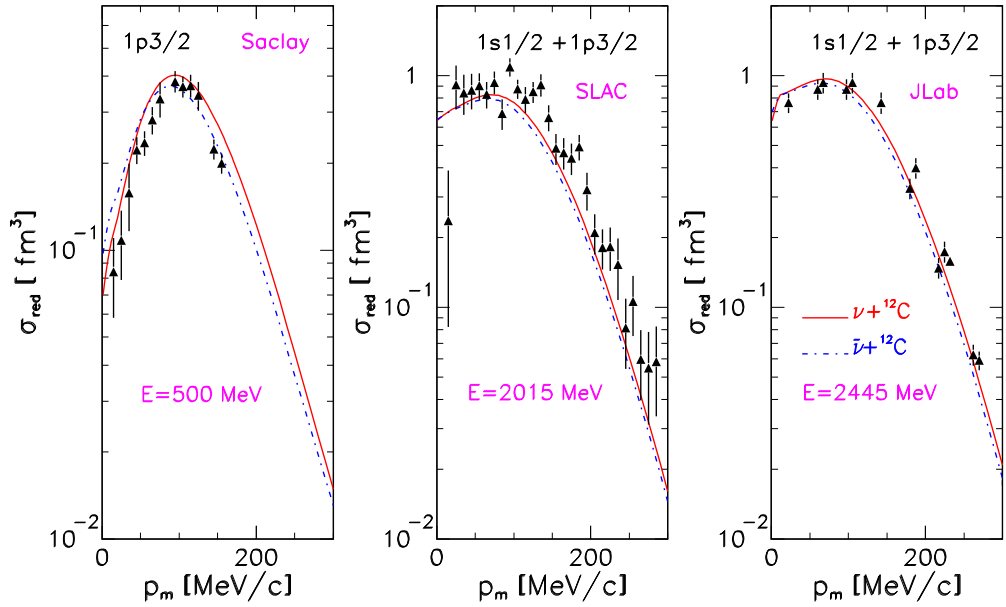

FIG. 5. The RDWIA calculation of neutrino (solid line) and antineutrino (dashed-dotted line) averaged reduced cross sections compared with measured exclusive cross section data for the removal of nucleons from $1p$ and $1s + 1p$ shells of ^{12}C as functions of the missing momentum. The data are from Saclay [53] for $1p$ and the beam energy $E_{\text{beam}} = 500$ MeV, from SLAC [56] for $1s + 1p$ shells and $E_{\text{beam}} = 2015$ MeV, and from JLab [41] for $1s + 1p$ shells and E_{beam}=2455 MeV.

IV. RESULTS AND ANALYSIS

The reduced cross sections of the ^{12}C$(e, e'p)$ reaction in the range of missing energy, that corresponds to knockout of $1s$- and $1p$-shell protons, were measured at Tokyo [52], Saclay [53,54], NIKHEF [55], SLAC [56], and JLab [41]. A review of analyses of the data [52–56] based upon the nonrelativistic distortion wave impulse approximation (NRDWIA) can be found in Ref. [57], which shows that spectroscopic factors for low-lying states are reduced relative to the IPSM by an average factor of about 65%. Most of the data contributing to the aforementioned estimate of 65% IPSM were limited to $Q^2 \leqslant 0.2$ (GeV/c)^2, and were analyzed using NRDWIA calculations based on empirical Woods-Saxon wave functions. Analysis the same low Q^2 data sets used in Ref. [57] based on the RDWIA with Dirac-Hartree wave functions was performed in Ref. [42]. This analysis is more accurate because it also includes the effects of distortion of lower components of Dirac spinors and takes into account overlap of single $1p$ and $1s$ nucleon energy distributions. It was found that the RDWIA calculation reproduces the low Q^2 data for quasiperpendicular kinematics well, but with same smaller normalization factors. For example, the $1p$ normalization factors for two Saclay experiments were 0.75 [53] and 0.63 [54] compared with 0.87 for the JLab data. The author argues that it should be attributed to the effective single-nucleon current operator instead of to spectroscopic factors, which are probe-independent properties of nuclear structure.

The knockout of $1p$-shell protons in ^{16}O$(e, e'p)$ was studied at Saclay [53,58], NIKHEF [59,60], Mainz [61], and JLab [46]. In these experiments, cross section data for the lowest-lying fragments of each shell were measured as functions of p_m, and normalization factors (relating how much the measured cross section data were less than predicted in IPSM) were extracted. The E12-14-012 experiment [62] performed in JLab measured the $(e, e'p)$ reduced cross sections using ^{40}Ar [63] and ^{48}Ti [64] targets. The reduced cross sections measured in the missing momentum and missing energy ranges $15 \leqslant p_m \leqslant 300$ MeV/c and $12 \leqslant E_m \leqslant 80$ MeV.

The distorted spectral function depends upon initial momentum $\boldsymbol{p}_m$, ejectile momentum $\boldsymbol{p}_x$, and angle between the initial and final nucleon momenta. Thus it depends upon kinematical conditions and is different for parallel and

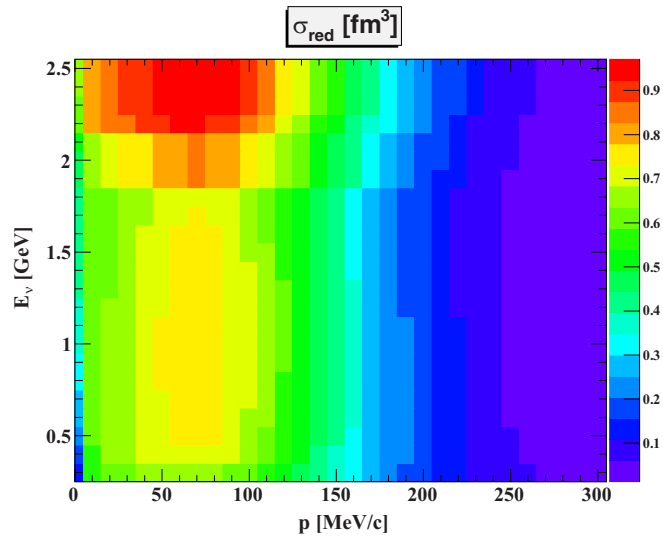

FIG. 6. The RDWIA neutrino averaged reduced cross section for removal of nucleons from the $1s + 1p$ shells of ^{12}C as a function of neutrino energy and missing momentum p_m.

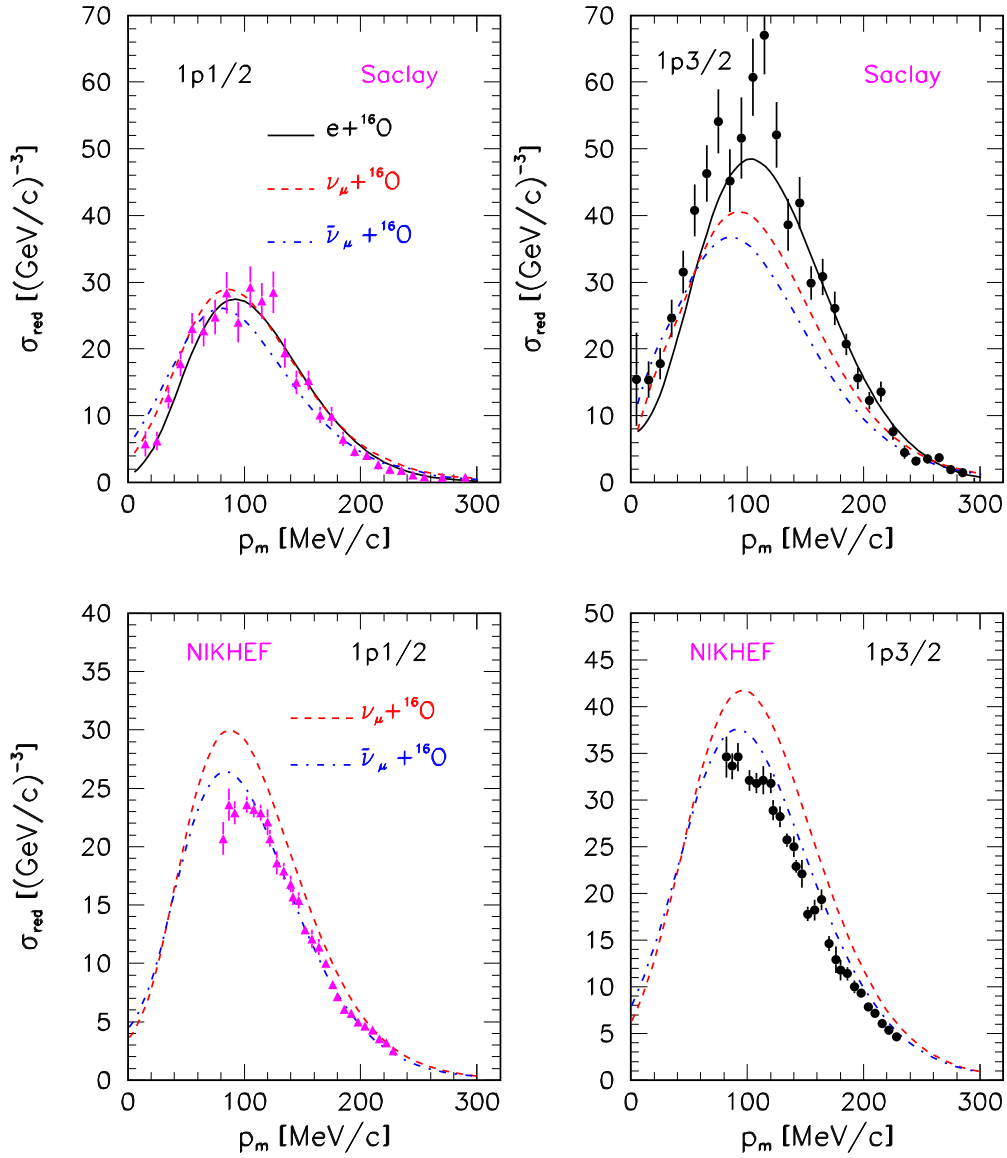

FIG. 7. Comparison of the RDWIA calculations for neutrino (dashed line) and antineutrino (dashed-dotted line) averaged reduced cross sections for the removal of nucleons from the $1p$ shell of ^{16}O with Saclay [53] and NIKHEF [59] data as functions of p_m. Also shown are the RDWIA calculations of the reduced cross section for electron scattering (solid line) from Ref. [7].

perpendicular kinematics. Furthermore, $\sigma_{\rm red}$ depends upon initial electron energy due to Coulomb distortion. The RDWIA approach with LEA code was successfully tested against measured ^{12}C$(e, e'p)$ [42], ^{16}O$(e, e'p)$ [46], and ^{40}Ca$(e, e'p)$ [12] differential and reduced cross sections, and the normalization factors $S(\alpha)$ for the IPSM orbitals were derived.

In Refs. [6,7,12] electron and CCQE (anti)neutrino scattering on oxygen, carbon, calcium, and argon targets were studied. It was found that the reduced cross sections for (anti)neutrino scattering are similar to those of electron scattering, and the latter are in good agreement with electron data. The difference between the electron and (anti)neutrino reduced cross sections calculated for Saclay kinematics is less than 10%. This can be attributed to Coulomb distortion of the electron wave function, which is usually described as the effective momentum approximation (EMA) [65]. In the EMA, the electron Coulomb wave function is replaced by a plane wave function with effective momentum whose value is larger than the value of electron momentum at infinity, because of Coulomb attraction. The flux is also increased in the interaction zone by focusing of electron wave. This effect is proportional to the charge of the target and weakens as the beam energy increases. The small difference between neutrino and antineutrino reduced cross sections is due to the difference in the FSI of the proton and neutron with the residual nucleus.

In this section I present the results of the RDWIA calculations of the averaged reduced cross sections, Eq. (10), for (anti)neutrino scattering off carbon, oxygen, and argon as functions of the missing momentum p_m and compare them with the measured $(e, e'p)$ reduced cross sections. In Ref. [7] electron, neutrino, and antineutrino cross sections for the removal of protons from the $1s$, $1p$, and $1s + 1p$ shells of ^{12}C

as functions of missing momentum p_m were calculated and compared with JLab data [41]. For illustration, Fig. 4 shows the measured removal cross sections as compared with the LEA code calculations [7]. It should be note that negative value of p_m corresponds to $\phi = \pi$ and positive to $\phi = 0$, where ϕ is the angle between the scattering $(\boldsymbol{k}_i, \boldsymbol{k}_f)$ and reaction $(\boldsymbol{p}_x, \boldsymbol{p}_B)$ planes. The data for beam energy $E_{\text{beam}} = 2.445$ GeV and $Q^2 = 0.64$ (GeV/c)^2 were measured in the quasiperpendicular kinematics with constant $(\omega, \boldsymbol{q})$. The electron and neutrino scattering off the nuclei are closely interrelated and one can treat both processes within the same formalism. There is an overall good agreement between the cross sections calculated in the RDWIA and data.

The averaged reduced cross sections for removal of nucleons from the $1p$, and $1s + 1p$ shells of $^{12}\text{C}(\nu_\mu, \mu p)$ and $^{12}\text{C}(\bar{\nu}_\mu, \mu n)$ reactions are shown in Fig. 5 as functions of positive p_m values together with Saclay [54], SLAC [42], and JLab [41] data. The data for beam energies $E_{\text{beam}} = 500$, 2015, and 2445 MeV were measured. There is an overall agreement between the calculated averaged cross sections and reduced cross sections of the $(e, e'p)$ reaction measured in different kinematics. The RDWIA averaged reduced cross section for removal of nucleons from $1s + 1p$ shells in $^{12}\text{C}(\nu_\mu, \mu p)$ is shown in Fig. 6 as a function of incoming neutrino energy and missing momentum p_m. In the range of the maximum at $60 \leqslant p_m \leqslant 90$ MeV/c the cross section increases slowly with neutrino energy, and slightly changes at $p_m \geqslant 120$ MeV/c and $p_m \leqslant 40$ MeV/c.

The averaged reduced cross sections for the removal of nucleons from the $1p$ shell in $^{16}\text{O}(\nu_\mu, \mu p)$ and $^{16}\text{O}(\bar{\nu}_\mu, \mu n)$ reactions are shown in Fig. 7 as functions of p_m, together with Saclay [53] and NIKHEF [59] data. There is an overall agreement between calculated cross sections and data, but the values of the calculated cross sections at maximum is systematically higher (about 15%) than measured ones for NIKHEF kinematics. Unfortunately, there are no data for removal of protons from the $1s$ and $1s + 1p$ shells of ^{16}O. Therefore the models of lepton-nucleus interaction that do not take into account the shell structure of the nucleus cannot be tested against the available reduced cross sections measured in the $^{16}\text{O}(e, e'p)$ reaction. As follows from the analysis in Ref. [46], a relativistic estimate of the model dependence of normalization factors for $^{16}\text{O}(e, e'p)$ reactions should not be less than ±15%. Although the relativistic model improves the description of A_{LT} asymmetry of the cross sections with $\phi = 0°$ and 180°, recoil polarization, and other normalization-independent features of the reaction, the model dependencies that affect the normalization uncertainty are not significantly improved. The RDWIA averaged reduced cross section for removal of nucleons from $1s + 1p$ shells in $^{16}\text{O}(\nu_\mu, \mu p)$ is shown in Fig. 8 as a function of incoming neutrino energy and missing momentum p_m. As can be seen from Figs. 6 and 8 the dependences of these cross sections upon neutrino energy and p_m are almost similar.

In Ref. [47] a coincidence electron-scattering experiment on ^{40}Ca at NIKHEF was performed. The spectral functions for missing momenta 0–280 MeV/c and excitation energies below 22 MeV were extracted. In an attempt to estimate the spectroscopic strength, a simple model where the spreading of

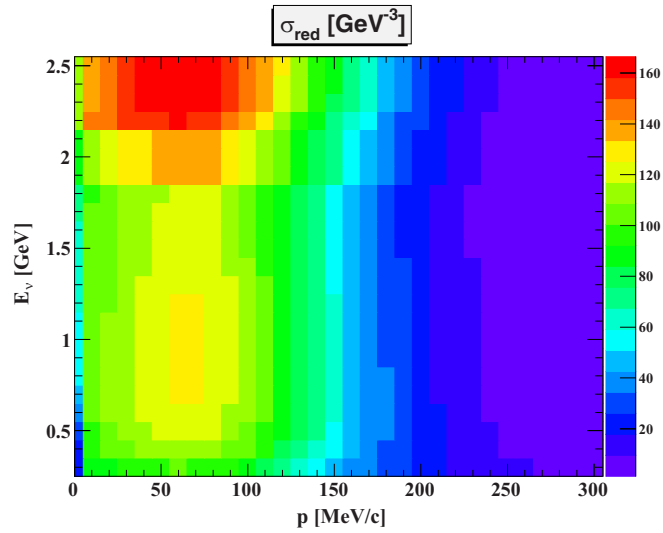

FIG. 8. Same as Fig. 6 but for ^{16}O.

the spectroscopic strength in missing energy is parametrized by a Lorentzian peak shape was used. Experimentally only the part residing between the Fermi level and the cutoff energy 35 MeV was detected. It was obtained that, although the exper-

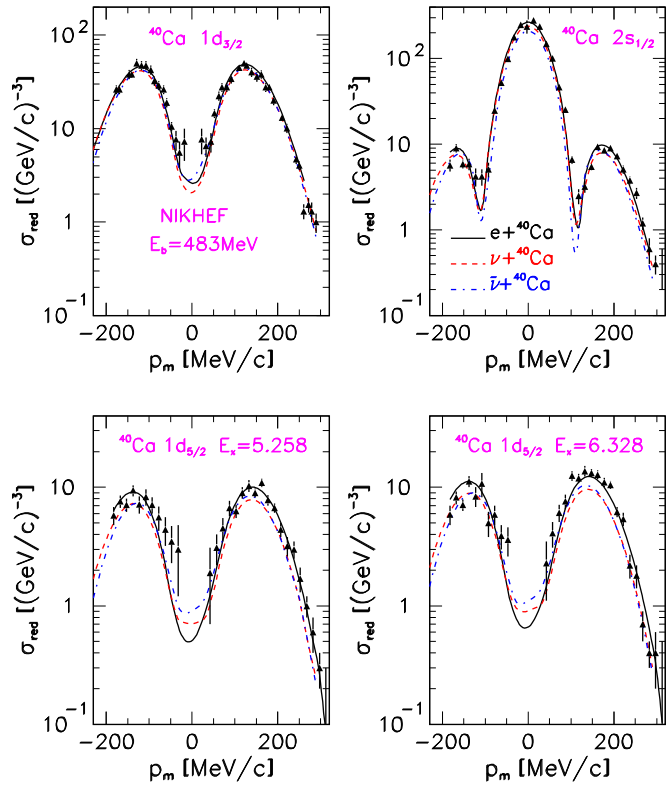

FIG. 9. Comparison of the RDWIA calculations for electron (solid line), neutrino (dashed line), and antineutrino (dashed-dotted line) reduced cross sections for the removal of nucleons from $1d_{3/2}$, $2s_{1/2}$, and $1d_{5/2}$ shells of ^{40}Ca with NIKHEF data [49]. The cross sections are presented as functions of missing momentum p_m. The figure was taken from Ref. [12].

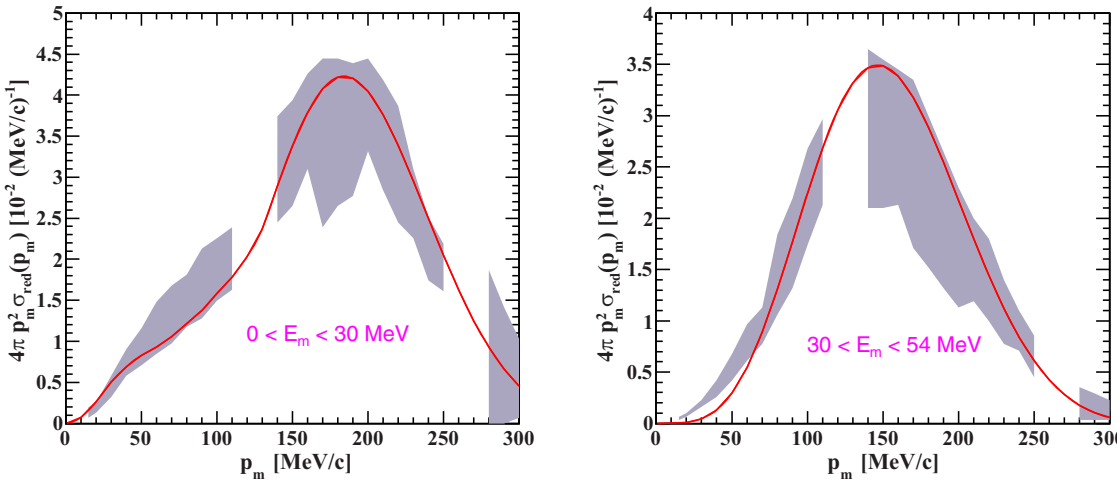

FIG. 10. Missing momentum distribution in argon obtained by integrating over the missing energy ranges of 0–30 MeV (left panel) and 30–54 MeV (right panel), presented with the geometrical factor of $4\pi\, p_m^2$. The gray band shows the measured spectral function including the full error.

imentally determined spectroscopic factors are on the order of 50% to 70% of the IPSM sum-rule limit, the extrapolated occupations of shell-model orbitals are about 90%. For ^{40}Ca the knockout from the $1s_{1/2}$ orbital was not observed in this experiment, but in Ref. [54] a spectroscopic factor of 1.5 for knockout from this orbital is given. The structures of calcium and argon nuclei are similar, although, unlike $^{40}_{18}$Ar, $^{40}_{20}$Ca is a symmetric and closed-shell nucleus. These features, and the different number of protons, introduce differences between the valence shells. However, for deeply bound states the peak positions turn out to agree to ≈ 2 MeV or better [63]. In Ref. [12] the $(e, e'p)$ reduced cross sections were calculated for removal of the proton from $1d_{3/2}$ shell, for transition to the $1/2^+$ exited state of the ^{39}K nucleus at excitation energy $E_x = 2.522$ MeV, and for the transitions to the $5/2^+$ excited states at $E_x = 5.258$ MeV and $E_x = 6.328$ MeV, obtained by knocking out protons from the $2s_{1/2}$ and $1d_{5/2}$ orbitals, respectively. The calculated reduced cross sections are shown in Fig. 9 with the NIKHEF data [47,48] and provide a good description of the shape and magnitude of the measured distribution. Neutrino and antineutrino calculated reduced cross sections of ^{40}Ca$(\nu, \mu^- p)^{39}$Ca and ^{40}Ca$(\bar{\nu}, \mu^+ n)^{39}$K reactions are also shown in Fig. 9. There is an overall good agreement between calculated cross sections, but the values of the electron cross sections at the maximum is systematically higher than those for (anti)neutrinos. This can be attributed to Coulomb distortion of the incident electron wave function.

The JLab experiment [62] measured the $(e, e'p)$ cross sections using argon and titanium targets [63,64]. The reduced cross sections were obtained in the missing momentum range $15 \leqslant p_m \leqslant 300$ MeV/c and missing energy range $12 \leqslant p_m \leqslant 80$ MeV. The procedure to obtain information on neutron distribution in argon is based on the observation that the neutron spectrum of $^{40}_{18}$Ar is mirrored by the proton spectrum of the nucleus of titanium, having charge $Z = 22$. Therefor one can expect that the proton spectral function obtained from Ti$(e, e'p)$ data provides information on the neutron spectral function of argon.

The $^{40}_{18}$Ar and $^{48}_{22}$Ti data were analyzed to obtain the spectral functions, describing the energy and momentum distributions of protons in the argon and titanium ground states. The effects of FSI, which are known to be significant in $(e, e'p)$ reactions, were taken into account within the distorted-wave impulse approximation approach. Figure 10 shows the missing momentum distributions of protons in argon obtained by integrating the data over the missing energy ranges 0–30 and 30–50 MeV. The proton missing momentum distribution in titanium was obtained by integrating the data over the missing energy range 0–30 MeV and is shown in Fig. 11. Also shown in Figs. 10 and 11 are the results obtained without FSI effects in the relativistic plane wave impulse approximation (RPWIA), with normalization factors S_α from Ref. [12]. There is an overall agreement between the RPWIA calculations and

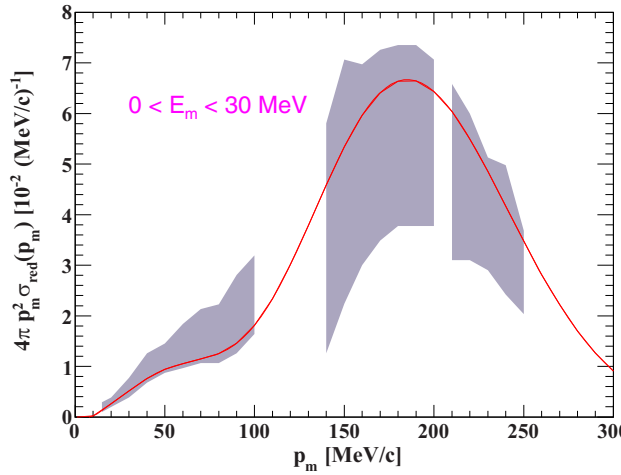

FIG. 11. Missing momentum distribution in titanium obtained by integrating over the missing energy range of 0–30 MeV, presented with the geometrical factor of $4\pi\, p_m^2$. The gray band shows the measured spectral function including the full error.

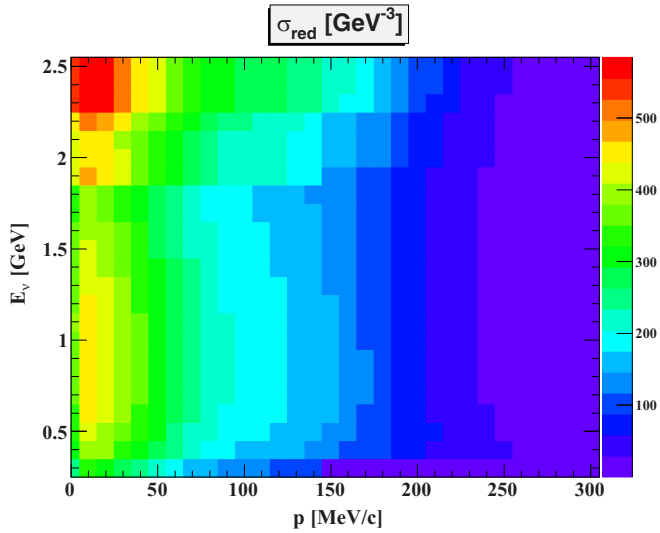

FIG. 12. Same as Fig. 6 but for ^{40}Ar.

data within sizable uncertainties of the measured proton momentum distributions. A more accurate determination of the distorted spectral functions for different shells of ^{40}Ar and ^{48}Ti will improve the testing of models using for description of neutrino interaction with these nucleus.

The averaged reduced cross section of the $^{40}\mathrm{Ar}(\nu_\mu, \mu p)$ reaction calculated in the RDWIA approach is shown in Fig. 12 as a function of neutrino energy and missing momentum p_m. It has to be pointed out that, unlike ^{12}C and ^{16}O, in ^{40}Ar the maximum of these cross sections is shifted to the range of lower missing momentum $p_m \approx 15$ MeV/c. The cross section increases very slowly with neutrino energy.

Neutrino event generators employ the factorization approach to make predictions about the lepton and also the outgoing nucleon kinematics from inclusive models. These models are aimed to describe an inclusive cross section that is only a function of the final lepton kinematics. This factorization uses the spectral functions, which are generated from different nucleon distributions in the initial nuclear state (local Fermi gas, shell model, etc). While the behavior of the cross section against the lepton kinematics may be described correctly, there is no guarantee that the correlations between the final lepton and nucleon for a given event are preserved. The comparison of the employed spectral function with the measured reduced cross sections allows the estimation of the accuracy of the nuclear effects calculations. On the other hand, the effective spectral functions can be obtained within the microscopic and unfactorized models, like the RDWIA, that successfully describe exclusive $(e, e'p)$ cross sections at large Q^2 and modest p_m.

In neutrino experiments [66] a subset of CCQE-like interactions (CC1$p0\pi$ interactions), includes CC-ν_μ ^{40}Ar scattering events with a detected muon and exactly one proton, with momenta greater than 100 and 300 (MeV/c) [$Q^2 \approx 0.1$ (GeV/c)^2], respectively. To improve description of the neutrino scattering data it would be necessary to apply a relativistic analysis to $(e, e'p)$ data for several values of Q^2 larger than about 0.1 (GeV/c)^2 and with sufficient coverage of p_m distributions to fit the wave functions. This would allow obtaining more precise normalization factors.

The reduced cross sections have been extensively studied by $(e, e'p)$ experiments carried out using a broad set of targets, ranging from carbon to calcium and argon. The accuracy of these data is significantly better than accuracy of the measured cross sections of the CC1$p0\pi$ interaction. To test the reliability and accuracy of the models used in the neutrino events generators, it is possible simulate (with only CCQE interaction) a set of CC1$p0\pi$ events at the kinematics of $(e, e'p)$ experiments, reconstruct the reduced cross section, and compare it with $(e, e'p)$ experimental data. This comparison will allows a better determination of the accuracy of the theoretical description of the quasielastic semiexclusive process of neutrino scattering off nuclei.

V. CONCLUSIONS

In this article, the semiexclusive reduced cross sections of CCQE (anti)neutrino scattering on carbon, oxygen, and argon were studied within the RDWIA approach. Averaged over phase space, reduced cross sections for removal of nucleons from the $1p$, and $1s + 1p$ shells of $^{12}\mathrm{C}(\nu_\mu, \mu p)$, $^{12}\mathrm{C}(\bar{\nu}_\mu, \mu n)$ and $^{16}\mathrm{O}(\nu_\mu, \mu p)$, $^{16}\mathrm{O}(\bar{\nu}_\mu, \mu n)$ reactions as functions of missing momentum and incoming neutrino energy were calculated and compared with the reduced cross sections obtained from measurements of $(e, e'p)$ scattering on ^{12}C and ^{16}O. I also calculated in the relativistic plane wave impulse approximation the averaged reduced cross sections for single nucleons knocked out in $^{40}\mathrm{Ar}(\nu_\mu, \mu p)$ and $^{49}\mathrm{Ti}(\bar{\nu}_\mu, \mu n)$ reactions as functions of p_m and ε_ν and compared them with proton momentum distributions in argon and titanium obtained from $(e, e'p)$ scattering in the JLab experiments.

I find that the shape and magnitude of the averaged reduced cross sections for (anti)neutrino scattering as a function of missing momentum are similar to measured reduced cross sections of electron scattering. The averaged removal cross sections calculated for argon and titanium within the RPWIA approach seem mostly consistent with the data within sizable uncertainties of measured proton momentum distributions. The difference of less than 10% between the electron and (anti)neutrino cross sections can be attributed to Coulomb distortion of the incoming electron wave function. The small difference between neutrino and antineutrino reduced cross sections is due to difference in the FSI of the proton and neutron with the residual nucleus. The averaged reduced cross sections for removal of nucleons from $1s + 1p$ shells in carbon and oxygen have a maximum in the range of missing momentum $60 \leqslant p_m \leqslant 90$ MeV/c, and in ^{40}Ar the maximum is shifted in the range of $p_m \approx 15$ MeV/c. The cross sections increase very slowly with neutrino energy.

Some neutrino event generators employ the factorization approach to make predictions about the lepton and outgoing nucleon kinematics, using different nucleon distributions in the ground nuclear state. In this way the direct comparison of the implemented spectral functions with the precise electron reduced cross section data allows one to estimate the accuracy of the nuclear effects calculations, such as the nuclear ground state and FSI.

ACKNOWLEDGMENTS

The author gratefully acknowledges A. Habig and S. Luchuk for fruitful discussions, constructive comments, and a critical reading of the manuscript.

[1] M. A. Acero *et al.* (NOvA Collaboration), Phys. Rev. Lett. **123**, 151803 (2019).
[2] K. Abe *et al.* (T2K Collaboration), Phys. Rev. Lett. **121**, 171802 (2018).
[3] R. Acciarri *et al.* (DUNE Collaboration), FERMILAB-DESIGN-2016-03, 2016.
[4] K. Abe *et al.* (Hyper-Kamiokande Collaboration), arXiv:1805.04163.
[5] R. Acciarri *et al.* (MicroBooNE, LAr1-ND, ICARUS-WA104 Collaboration), arXiv:1503.01520.
[6] A. V. Butkevich and S. A. Kulagin, Phys. Rev. C **76**, 045502 (2007).
[7] A. V. Butkevich, Phys. Rev. C **80**, 014610 (2009).
[8] M. Martini, M. Ericson, and G. Chanfray, Phys. Rev. C **84**, 055502 (2011).
[9] M. Martini and M. Ericson, Phys. Rev. C **87**, 065501 (2013).
[10] J. Nieves, I. Ruiz Simo, and M. J. Vicente Vacas, Phys. Lett. B **707**, 72 (2012).
[11] J. Nieves, I. Ruiz Simo, and M. J. Vicente Vacas, Phys. Lett. B **721**, 90 (2013).
[12] A. V. Butkevich, Phys. Rev. C **85**, 065501 (2012).
[13] M. Martini, N. Jachowicz, M. Ericson, V. Pandey, T. Van Cuyck, and N. Van Dessel, Phys. Rev. C **94**, 015501 (2016).
[14] I. Ruiz Simo, J. E. Amaro, M. B. Barbaro, A. De Pace, and J. A. Caballero, J. Phys. G **44**, 065105 (2017).
[15] G. D. Megias, T. W. Donnelly, O. Moreno, C. F. Williamson, J. A. Caballero, R. Gonzalez-Jimenez, A. De Pace, M. B. Barbaro, W. M. Alberico, M. Nardi, and J. E. Amaro, Phys. Rev. D **91**, 073004 (2015).
[16] G. D. Megias, J. E. Amaro, M. B. Barbaro, J. A. Caballero, and T. W. Donnelly, Phys. Rev. D **94**, 013012 (2016).
[17] G. D. Megias, J. E. Amaro, M. B. Barbaro, J. A. Caballero, T. W. Donnelly, and I. R. Simo, Phys. Rev. D **94**, 093004 (2016).
[18] N. Rocco, C. Barbieri, O. Benhar, A. De Pace, and A. Lovato, Phys. Rev. C **99**, 025502 (2019).
[19] A. V. Butkevich and S. V. Luchuk, Phys. Rev. C **97**, 045502 (2018).
[20] A. V. Butkevich and S. V. Luchuk, Phys. Rev. D **99**, 093001 (2019).
[21] M. B. Barbaro, J. A. Caballero, A. De Pace, T. W. Donnelly, R. Gonzalez-Jimenez, and G. D. Megias, Phys. Rev. C **99**, 042501(R) (2019).
[22] R. Gonzalez-Jimenez, A. Nikolakopoulos, N. Jachowicz, and J. M. Udias, Phys. Rev. C **100**, 045501 (2019).
[23] R. Gonzalez-Jimenez, M. B. Barbaro, J. A. Caballero, T. W. Donnelly, N. Jachowicz, G. D. Megias, K. Niewczas, A. Nikolakopoulos, and J. M. Udias, Phys. Rev. C **101**, 015503 (2020).
[24] A. V. Butkevich and S. V. Luchuk, Phys. Rev. C **102**, 024602 (2020).
[25] A. V. Butkevich, Phys. Rev. C **105**, 025501 (2022).
[26] A. V. Butkevich, Phys. Rev. D **107**, 073001 (2023).
[27] K. S. Kim, S. Choi, T. Miyatsu, M. K. Cheoun, H. Kim, and W. Y. So, Phys. Rev. C **107**, 024607 (2023)
[28] M. Khachatryan, A. Papapdopoulou, A. Ashkenazi, F. Hauenstein, L. B. Weinstein, O. Hen, E. Piasetzky *et al.* (CLAS and e4v Collaboration), Nature (London) **599**, 565 (2021).
[29] A. Picklesimer, J. W. Van Orden, and S. J. Wallace, Phys. Rev. C **32**, 1312 (1985).
[30] J. M. Udias, P. Sarriguren, E. Moya de Guerra, E. Garrido, and J. A. Caballero, Phys. Rev. C **51**, 3246 (1995).
[31] James J. Kelly, Phys. Rev. C **59**, 3256 (1999).
[32] A. M. Ankowski and A. Friedland, Phys. Rev. D **102**, 053001 (2020).
[33] A. Papadopoulou *et al.* (e4v Collaboration), Phys. Rev. D **103**, 113003 (2021).
[34] S. Dolan, J. McElwee, S. Bolognesi, Y. Yayato, K. McFarland, G. Megias, K. Nlewczas, L. Pickering, J. Sobczyk, L. Tompson, and G. Wret, arXiv:2301.09195.
[35] S. Dytman, Y. Hayato, R. Raboanary, J. T. Sobczyk, J. Tena Vidal, and N. Vololoniaina, Phys. Rev. D **104**, 053006 (2021).
[36] A. Nikolakopoulos, R. Gonzalez-Jimenez, N. Jachowicz, K. Niewczas, F. Sanchez, and J. M. Udias, Phys. Rev. C **105**, 054603 (2022).
[37] T. de Forest, Nucl. Phys. A **392**, 232 (1983).
[38] P. Mergell, U.-G. Meissner, and D. Drechsel, Nucl. Phys. A **596**, 367 (1996).
[39] B. D. Serot and J. D. Walecka, Adv. Nucl. Phys. **16**, 1 (1986).
[40] C. J. Horowitz D. P. Murdock, and Brian D. Serot, in *Computational Nuclear Physics 1: Nuclear Structure*, edited by K. Langanke, J. A. Maruhn, and S. E. Koonin (Springer-Verlag, Berlin, 1991), p. 129.
[41] D. Dutta *et al.*, Phys. Rev. C **68**, 064603 (2003).
[42] J. J. Kelly, Phys. Rev. C **71**, 064610 (2005).
[43] D. Rohe *et al.*, Nucl. Phys. B **159**, 152 (2006).
[44] T. Frick, K. S. A. Hassaneen, D. Rohe, and H. Müther, Phys. Rev. C **70**, 024309 (2004).
[45] O. Benhar, A. Fabrocini, and S. Fantoni, Phys. Rev. C **41**, R24 (1990).
[46] K. G. Fissum *et al.*, Phys. Rev. C **70**, 034606 (2004).
[47] G. J. Kramer, https://inis.iaea.org/search/search.aspx?orig_q=RN:22024922.
[48] G. J. Kramer *et al.*, Phys. Lett. B **227**, 199 (1989).
[49] G. J. Kramer, H. P. Blok, and L. Lapikas, Nucl. Phys. A **679**, 267 (2001).
[50] J. J Kelly, http://www.physics.umd.edu/enp/jjkelly/LEA.
[51] E. D. Cooper, S. Hama, B. C. Clark, and R. L. Mercer, Phys. Rev. C **47**, 297 (1993).
[52] K. Nakamura and N. Izutsu, Nucl. Phys. A **259**, 301 (1976).
[53] M. Bernheim *et al.*, Nucl. Phys. A **375**, 381 (1982).
[54] J. Mougey, M. Bernheim, A. Bussiere, A. Gillebert, P. X. Ho, M. Priou, D. Royer, I. Sick, and G. Wagner, Nucl. Phys. A **262**, 461 (1976).
[55] G. van der Steenhoven, H. P. Block, E. Jans, M. de Jong, L. Lapikas, E. N. Quint, and P. K. A. Witt Huberts, Nucl. Phys. A **480**, 547 (1988).

[56] N. C. R. Makins, R. Ent, M. S. Chapman, J. O. Hansen, K. Lee, R. G. Milner *et al.*, Phys. Rev. Lett. **72**, 1986 (1994).
[57] L. Lapikas, G. van der Steenhoven, L. Frankfurt, M. Strikman, and M. Zhalov, Phys. Rev. C **61**, 064325 (2000).
[58] L. Chinitz, M. Bernheim, G. P. Capitani, A. Catarinella, J. F. Danel, E. DeSanctis *et al.*, Phys. Rev. Lett. **67**, 568 (1991).
[59] K. I. Blomqvist *et al.*, Phys. Lett. B **344**, 85 (1995).
[60] M. Leuschner *et al.*, Phys. Rev. C **49**, 955 (1994).
[61] K. I. Blomqvist *et al.*, Z. Phys. A **351**, 353 (1995).
[62] L. Gu *et al.* (Jefferson Lab HAll A Collaboration), Phys. Rev. C **103**, 034604 (2021).
[63] L. Jiang *et al.* (Jefferson Lab HAll A Collaboration), Phys. Rev. D **105**, 112002 (2022).
[64] L. Jiang *et al.* (Jefferson Lab HAll A Collaboration), Phys. Rev. D **107**, 012005 (2023).
[65] L. L. Schiff *et al.*, Phys. Rev. **103**, 443 (1956).
[66] P. Abratenko *et al.* (MicroBooNE Collaboration), Phys. Rev. Lett. **125**, 201803 (2020).